Title

From Sugars to Wheels: The Conversion of Ethanol to 1,3-Butadiene over Metal-Promoted Magnesia-Silicate Catalysts

Journal

ChemSusChem, 9(12)

ISSN

1864-5631

Authors

Shylesh, Sankaranarayanapillai
Gokhale, Amit A
Scown, Corinne D
et al.

Publication Date

2016-06-22

DOI

10.1002/cssc.201600195

Peer reviewed

ChemPubSoc Europe

DOI: 10.1002/cssc.201600195

CHEMSUSCHEM Full Papers

From Sugars to Wheels: The Conversion of Ethanol to 1,3-Butadiene over Metal-Promoted Magnesia-Silicate Catalysts

Sankaranarayanapillai Shylesh,[a, e] Amit A. Gokhale,[a, b] Corinne D. Scown,[a, c, d] Daeyoup Kim,[e] Christopher R. Ho,[e] and Alexis T. Bell*[a, e]

1,3-Butadiene (1,3-BD) is a high-value chemical intermediate used mainly as a monomer for the production of synthetic rubbers. The ability to source 1,3-BD from biomass is of considerable current interest because it offers the potential to reduce the life-cycle greenhouse gas (GHG) impact associated with 1,3-BD production from petroleum-derived naphtha. Herein, we report the development and investigation of a new catalyst and process for the one-step conversion of ethanol to 1,3-BD. The catalyst is prepared by the incipient impregnation of magnesium oxide onto a silica support followed by the deposition of Au nanoparticles by deposition–precipitation. The resulting Au/MgO-SiO_2 catalyst exhibits a high activity and selectivity to 1,3-BD and low selectivities to diethyl ether, ethylene, and butenes. Detailed characterization of the catalyst shows that the desirable activity and selectivity of Au/MgO-SiO_2 are a consequence of a critical balance between the acidic–basic sites associated with a magnesium silicate hydrate phase and the redox properties of the Au nanoparticles. A process for the conversion of ethanol to 1,3-BD, which uses our catalyst, is proposed and analyzed to determine the life-cycle GHG impact of the production of this product from biomass-derived ethanol. We show that 1,3-BD produced by our process can reduce GHG emissions by as much as 155% relative to the conventional petroleum-based production of 1,3-BD.

Introduction

Over the past decade, growing consumer awareness and the desire to reduce carbon emissions have driven an increase in the demand for chemicals sourced sustainably.[1] Bio-based chemicals have the potential to meet this renewable chemical demand and reduce greenhouse gas (GHG) emissions substantially.[2] Of all the biomass-derived intermediates that can serve as building blocks for the chemical industry, ethanol is particularly attractive because it can be used for the direct production of chemicals such as ethylene, propylene, and 1,3-butadiene (1,3-BD), as well as oxygen-containing molecules such as 1-butanol, ethyl acetate, and acetic acid.[3] Of these products, 1,3-BD deserves particular attention because it is a high-value added chemical intermediate used for the production of synthetic rubbers and other polymers. The primary use for 1,3-BD is to produce styrene-butadiene rubber (SBR) and polybutadiene, which consume 28 and 26%, respectively, of the global demand for 1,3-BD.[4] 1,3-BD also finds application in the production of acrylonitrile-butadiene-styrene (ABS; 12%), styrene-butadiene latex (12%), chloroprene rubber (2%), and adiponitrile, a precursor for nylon (6%).[5,6]

The catalytic conversion of ethanol to 1,3-butadiene (ETB) is an industrially proven technology practiced from the 1920s through the late 1960s. The two ETB processes of particular interest were a one-step process developed by Lebedev, which used a variety of basic mixed oxide catalysts, and a two-step process known as the Ostromislensky process, which used tantalum oxide-silica catalysts and was commercialized in the USA by Union Carbide and the Carbon Chemical Corporation.[7–9] Both processes became economically uncompetitive after the 1960s because of the development of routes to 1,3-BD based on petroleum-derived naphtha. Currently, approximately 95% of 1,3-BD is a coproduct of ethylene production isolated by the extractive distillation of C_4 fractions from naphtha steam crackers.[3] The problem with this approach is that the C_4 fraction contains a mixture of butadiene, butane, and butenes, compounds that are difficult to separate because they form azeotropes. Extractive distillation is the only viable option to separate butadiene from the C_4 fractions using solvents such as *N*-methylpyrrolidone, dimethylformamide, and acetoni-

[a] Dr. S. Shylesh, Dr. A. A. Gokhale, Dr. C. D. Scown, Prof. A. T. Bell
Energy Biosciences Institute
University of California
2151 Berkeley Way, Berkeley, CA 94720 (USA)
E-mail: alexbell@berkeley.edu

[b] Dr. A. A. Gokhale
BASF Corporation
33 Wood Avenue South, Iselin, NJ 08830 (USA)

[c] Dr. C. D. Scown
Joint BioEnergy Institute
5885 Hollis Street, Berkeley, CA 94608 (USA)

[d] Dr. C. D. Scown
Energy Technologies Area
Lawrence Berkeley National Laboratory
Berkeley, CA 94720 (USA)

[e] Dr. S. Shylesh, D. Kim, C. R. Ho, Prof. A. T. Bell
Department of Chemical and Biomolecular Engineering
University of California
Berkeley, CA 94720 (USA)

Supporting Information for this article can be found under: http://dx.doi.org/10.1002/cssc.201600195.

trile.[10] Although these solvents allow the separation of alkenes from butadiene, alkynes that are also present in the C_4 petroleum fraction cannot be separated efficiently. Consequently, additional separations are needed to meet the tight specification of <40 ppm acetylenes for polymer-grade butadiene, which makes the recovery process quite GHG intensive.[11]

The demand–supply dynamics for butadiene also motivate efforts to develop alternative sources. The supply of butadiene is tied to ethylene crackers and the feedstocks that are used to produce ethylene, and on-purpose butadiene production, although technically possible, is virtually nonexistent. Consequently, in certain periods the demand for butadiene drives the spot price as high as ~$4740/ton, as in August 2011, and at other times the prices can dip to as low as $685/ton, as was the case in May 2015.[12] The highly reactive nature of butadiene prevents producers and consumers from holding large inventories and hence disturbances in the ethylene supply chain tend to affect butadiene markets significantly. This trend has been exacerbated by the recent shale gas surge; ethylene can be produced cheaply by the dehydrogenation of ethane, but this process yields very little or no 1,3-BD.[13,14] These factors have led to serious supply shortages at times and the overall volatility of the butadiene market has stimulated the development of alternate technologies for the on-purpose production of 1,3-BD.

Recent research indicates that the direct production of butadiene is achievable through a variety of routes, which include the condensation of ethanol to 1,3-BD, dehydration of 1,4-butanediol and 1,3-butanediol, and dehydrogenation of butane and butenes.[13] Today, the global production of ethanol amounts to more than 100 billion liters, which is an order of magnitude higher than the 1,3-BD demand.[3] Thus the one-step conversion of ETB is becoming more attractive as a potential alternative to the production of 1,3-BD from naphtha. For example, a recent high-level risk and uncertainty-based sustainability assessment by Patel et al. suggests that the bioethanol-based production of 1,3-BD may have value over the conventional naphtha cracking process.[15] In this report, we propose to take the analysis a step further and develop the right type of heterogeneous catalysts to convert ethanol into butadiene effectively. This catalyst is then used in a proposed ETB process and the process is analyzed to determine the life-cycle GHG impact This analysis reveals that although the trends developed from high-level analysis are valuable, the details of the local factors such as geographic location and utility sources can play a significant role to influence the overall GHG impact.

Several research groups have investigated the use of magnesia-silica ($MgO\text{-}SiO_2$) catalysts for the single-step conversion of ETB. These studies have typically reported 1,3-BD yields of 10–30%.[16–19] Catalytic activity has been linked to the method of catalyst preparation by techniques as divergent as kneading MgO with colloidal silica followed by calcination to the use of sepiolite, a fibrous magnesia-silica clay mineral.[20,21] Although MgO can catalyze aldol condensation and SiO_2 provides the acid sites necessary for dehydration, the addition of transition metals improves the dehydrogenation of ethanol to acetaldehyde. For example, Jones et al. have shown that at 648 K a maximum butadiene selectivity of 60% could be achieved using Cu/Zr/Zn oxide supported on silica.[22] Very recently, Makshina et al. have shown that magnesia-silica-supported Ag and Cu are active catalysts for ETB with butadiene yields greater than 40% at 673 K.[3,23] Similarly, Sushkevich et al. claimed that Ag supported on zirconia-silica is an active catalyst for the production of 1,3-BD with 1,3 BD yields of 40% at a weight hourly space velocity (WHSV) of 0.3 h^{-1} and 593 K.[24,25] Despite these advances, the attainment of a high selectivity to 1,3-BD in a one-step process together with a high ethanol conversion at high ethanol partial pressures has proven to be challenging, primarily because of the formation of undesirable byproducts, particularly butenes, which are difficult to separate from butadiene and would contribute to high GHG emissions if these catalysts were used in a process.[11]

In this work, we demonstrate that a catalyst that comprises Au dispersed on magnesium silicate hydrate (MSH) formed by the reaction of MgO and silica shows a high activity and selectivity to 1,3-BD at a low temperature (573 K) and a high partial pressure of ethanol (~20 kPa). Under these conditions, it was possible to achieve an ethanol conversion of up to 60% and a 1,3-BD yield of 47% with only 2% conversion of ethanol to butenes and 8% ethanol conversion to ethylene and no production of diethyl ether and acetylene. By contrast, Sels et al. have reported the formation of diethyl ether and other C_4 hydrocarbon and oxygenated byproducts in more than 25% selectivity at 673 K using a Ag supported on magnesia-silica catalyst.[5] Diethyl ether is known to form azeotropes with ethanol as well as acetaldehyde, which complicates the separation of 1,3-BD from ethanol-derived butadiene considerably, and the presence of alkynes in 1,3-BD is known to create problems with the storage, transport, and subsequent polymerization of the product. We show that the high activity and selectivity to 1,3-BD exhibited by our catalyst is a consequence of the nature of the metal and of the composition, structure, and textural properties of the support.

To explore the environmental benefits of the use of our catalyst, we propose a process for the conversion of biomass-based ETB and perform a life-cycle analysis of the GHG emission of the process for several geographically specific scenarios. The findings of this analysis are compared with the GHG emissions produced by a process based on the use of petroleum-sourced naphtha as the feedstock. We show that, after accounting for biogenic carbon sequestration associated with landfilling and other noncombustion fates for bio-based butadiene in rubber products, the GHG impact of butadiene produced by our process is highly dependent on the source of ethanol. The use of Brazilian sugarcane ethanol or ethanol derived from American corn stover is predicted to produce 1,3-BD with a net carbon-negative GHG footprint. The life-cycle GHG footprint can ultimately be reduced by as much as 155% relative to conventional petroleum-based 1,3-BD. However, we find that the use of ethanol derived from corn starch results in increased GHG emissions for the production of 1,3-BD compared to that of the production of 1,3-BD from petroleum.

Results and Discussion

Characterization

XRD patterns of SiO_2, MgO-SiO_2, and MgO-SiO_2-supported Au are shown in Figure 1 and compared with the diffraction pattern of crystalline MgO. For MgO loadings between 10 and 50 wt%, no peaks for crystalline MgO were observed (Figure S1). For 50 wt% MgO-loaded SiO_2, broad peaks of MgO

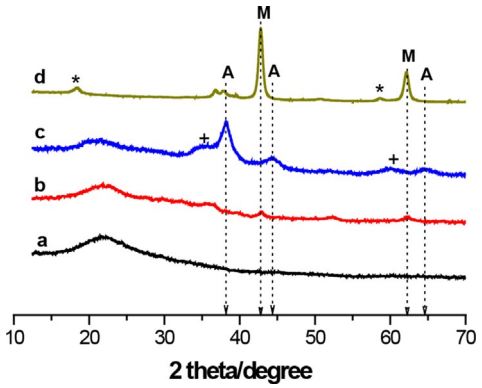

Figure 1. XRD patterns of a) SiO_2, b) 50%MgO-SiO_2, c) ~3%Au/50%MgO-SiO_2, and d) MgO. M = periclase MgO, A = metallic Au, + = MSH, * = $Mg(OH)_2$.

could be seen, suggestive of low crystallinity because of the small size of the MgO crystals, and new peaks appeared at $2\theta = 33–40^\circ$ because of the formation of a MSH phase.[5,26,27] An increase of the MgO loading to 80 wt% resulted in the formation of crystalline MgO. The diffraction peaks observed at $2\theta = 36.9$, 42.7, and 62.3° correspond to the face-centered cubic (fcc) form of MgO (periclase). After the deposition of Au (5–6 nm), we observed new peaks that correspond to metallic Au at $2\theta = 38$, 44.5, and 64.5°.[28] Interestingly, after the deposition of Au on 50–80 wt% MgO-SiO_2, a complete disappearance of the peaks of the MgO phase and the formation of a corresponding MSH phase is observed (Figure 1 and Figure S2). We hypothesize that the formation of MSH after Au deposition is a consequence of the presence of water and the use of high temperatures during the deposition–precipitation (DP) procedure.

^{29}Si magic-angle spinning (MAS) NMR spectroscopy was used to evaluate the environment of the Si atoms for various loadings of MgO and to confirm the formation of a magnesia-silicate phase at higher MgO loadings (Figure 2). The support silica exhibited Q^3 and Q^4 peaks at $\delta = -100$ and -110 ppm, respectively. The Q^3 feature is caused by silanol groups [Si*$(OSi)_3(OH)$], whereas the Q^4 feature is because of Si atoms coordinated to four other Si atoms through Si–O–Si bonds [Si*$(OSi)_4$].[5,26,29] The absence of Q^2 Si atoms [Si*$(OSi)_2(OH)_2$] at $\delta = -90$ ppm shows that the presence of geminal silanol groups on the silica support surface is negligible. Q^4 Si features are present together with very few Q^3 features for catalysts that contain 10 and 30 wt% MgO, which suggests that these catalysts retain the properties of the support SiO_2. On these

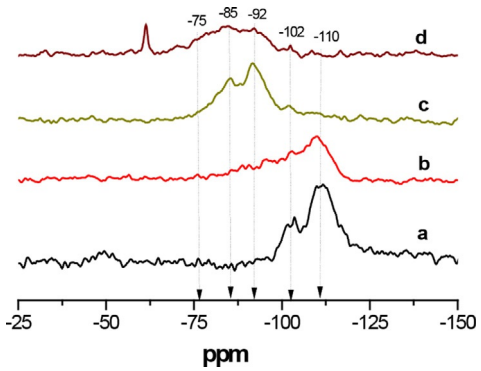

Figure 2. ^{29}Si MAS NMR spectra of Au doped various samples: a) SiO_2, b) 10%MgO-SiO_2, c) 50%MgO-SiO_2, and d) 80%MgO-SiO_2.

catalysts, Mg^{2+} cations interact primarily with the isolated silanol groups.[5] Interestingly, the addition of 50–80 wt% MgO to the silica support led to the complete disappearance of the Q^4 and Q^3 resonances of the support silica and the appearance of new peaks at $\delta = -92$, -85, and -75 ppm related to the formation of [Si*$(OMg)(OSi)_3$], [Si*$(OMg)(OSi)_2(OH)$], and [Si* $(OMg)_2(OSi)_2$], respectively.[5,26,29] These observations confirm that for MgO loadings at or above 50 wt%, the support transforms to MSH.

The elemental maps obtained by scanning transmission electron microscopy with energy-dispersive spectroscopy (STEM-EDS; Figure 3) display a uniform distribution of Mg and Si,

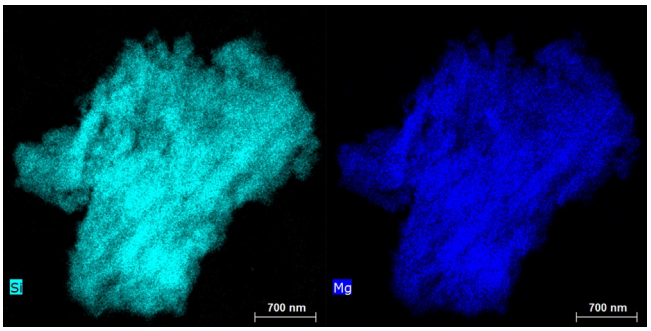

Figure 3. Elemental maps of Si and Mg obtained by STEM-EDS for ~3%Au/50%MgO-SiO_2 that show the intimate mixing of Si and Mg.

which further supports the idea that upon calcination, the magnesium precursor forms magnesia-silicate rather than bulk MgO particles if the Mg/Si ratio is greater than 2. The formation of this phase is thought to be a consequence of the thin pore walls of the silica, which undergo the disruption of the Si–O–Si bonds and the interaction of the resulting Si–OH groups with the magnesium precursor to form the MSH phase in the presence of water and HCl produced from the hydrolysis of $HAuCl_4$ during the DP procedure. This hypothesis is supported by the work of Israelachvili and co-workers who point out that in the presence of water, the surface of silica is reconstructed to form polymeric hydroxylated chains that act as silicic acid.[30] These species are reactive towards the hydrolysable

magnesium cations to lead to the formation of hydrated magnesium silicate. The role of water and acid to promote the formation of strong Si–O–Mg bonds is supported by the failure to observe an MSH phase if a physical mixture of MgO and SiO_2 is calcined at 823 K in the absence of water. In this case, only sharp peaks for crystalline MgO were observed, which suggests that the formation of the MSH phase is aided by the presence of water. Consistent with this result, we found that the use of $Au(acetate)_3$ as a precursor instead of $HAuCl_4$ did not lead to any changes in the MgO-SiO_2 sample or to the formation of MSH. However, the treatment of MgO-SiO_2 with an aqueous solution of HCl results in the formation of the MSH phase. All these results allow us to propose that the DP procedure and the use of $HAuCl_4$ as the precursor enhance the formation of the MSH phase.

To characterize the basic sites present on the catalyst surface, in situ IR spectroscopy was performed over the silica-supported MgO catalysts using CO_2 as a probe molecule. The IR spectra obtained after CO_2 adsorption at room temperature and after subsequent desorption at 473 K are shown in Figure 4. As expected, the silica support did not adsorb CO_2,

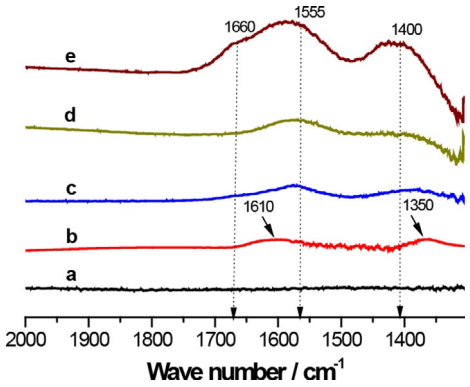

Figure 4. IR spectra of CO_2 adsorbed on a) SiO_2, b) 10%MgO-SiO_2, c) 30%MgO-SiO_2, d) 50%MgO-SiO_2, and e) 80%MgO-SiO_2.

which shows the absence of basic sites. Three different forms of adsorbed CO_2 were observed on MgO-SiO_2, which reflects three different types of basic sites on the catalyst surface. The bands at $\tilde{\nu}$ = 1560–1510 and 1400–1360 cm^{-1} are attributable to the asymmetric and symmetric O–C–O stretching vibrations, respectively, of unidentate carbonate species formed on high-strength basic sites (O^{2-}).[31] CO_2 adsorption on Mg–O pairs that have a medium basicity produce bidentate carbonate species that have characteristic asymmetric and symmetric O–C–O vibrations near $\tilde{\nu}$ = 1630–1610 and 1350–1320 cm^{-1}. Finally, bicarbonate species formed by the reaction of CO_2 with weakly basic surface hydroxyl groups exhibit asymmetric and symmetric O–C–O stretching vibrations at $\tilde{\nu}$ = 1670–1650 and 1480–1420 cm^{-1}, respectively. Medium-strength basic sites predominate at low magnesium loadings (10–30 wt%) and the relative proportion of strongly basic sites (peaks at $\tilde{\nu} \approx 1555$ and 1400 cm^{-1}) increases with the MgO loading (Figure 4). Importantly, a new peak appears for 50–80 wt% MgO at $\tilde{\nu}$ = 1660 cm^{-1}, which indicates the presence of bicarbonate species formed on low-strength basic sites.[5] The desorption of CO_2 by increasing the temperature above 473 K results in a complete disappearance of the bicarbonate species attached to weakly basic sites; however, unidentate and bidentate carbonate species remained on the surface up to 573 K. After evacuation at 623 K, only unidentate carbonate species were detected, which suggests the presence of high-strength basic sites on the surface of the magnesia-silicate.

The acidic properties of the magnesia-silica catalysts were characterized by IR spectroscopy using adsorbed pyridine as a probe. In general, IR peaks at $\tilde{\nu}$ = 1445 and 1605 cm^{-1} indicate the presence of strong Lewis acid sites (L); peaks at $\tilde{\nu}$ = 1490 cm^{-1} correspond to a combination of Lewis and Brønsted acid sites (L+B); a peak at $\tilde{\nu}$ = 1540 cm^{-1} indicates Brønsted acid sites (B); and the peak at $\tilde{\nu}$ = 1590 cm^{-1} shows hydrogen-bound pyridine (H).[32,33] IR spectra recorded after pyridine adsorption at room temperature and subsequent desorption at 473 K (Figure S3) suggest that the magnesia-silica contains strong Lewis acid sites and no Brønsted acid sites. The absence of Brønsted acidic sites on these catalysts suggests that the residual silanol groups present on the support are only weakly acidic. The presence of sharp bands at $\tilde{\nu}$ = 1445 and 1605 cm^{-1} for adsorbed pyridine indicates the presence of Lewis acid sites on magnesia-silica.

Catalyst activity and selectivity

The effects of MgO loading on the activity and selectivity of silica-supported MgO are illustrated in Figure 5. The conversion of ethanol at 573 K decreases with the increasing MgO loading. At low MgO loadings, the principal product is ethylene, and with an increasing MgO loading the selectivity to ethylene decreases and the selectivities to acetaldehyde and 1,3-BD increase monotonically. These results suggest that although MgO catalyzes aldol condensation, its activity is much lower than that of the silanol groups present on silica, which catalyze ethanol dehydration to ethylene. This result is further supported by studies that show that the cofeeding of acetaldehyde to-

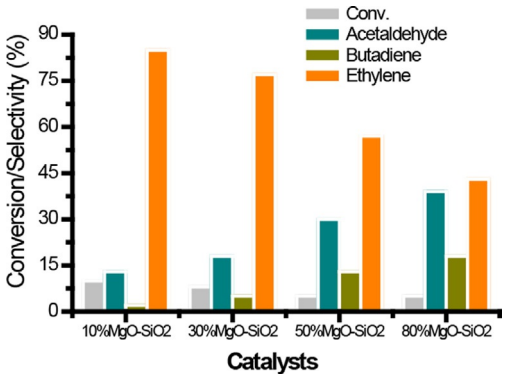

Figure 5. Effect of MgO loading on the activity and selectivity of MgO-SiO_2 for ethanol conversion to 1,3-BD. Reaction conditions: T = 573 K, WHSV = 1.1 h^{-1}, Q_{tot} = 20 $cm^3 min^{-1}$, $P_{ethanol}$ = ~20 kPa, M_{cat} = 0.3 g.

gether with ethanol leads to an approximately fourfold increase in the rate of 1,3-BD formation over MgO-SiO_2.[18,20]

We hypothesized that as the dehydrogenation of ethanol to acetaldehyde is a crucial step in the ETB sequence, the deposition of redox metals on magnesia-silicates would enhance the ethanol conversion and selectivity towards 1,3-BD.[3] Among the different redox metals evaluated, Au showed a much higher selectivity to 1,3-BD than Ag, Pd, and Cu (Table S1). Au nanoparticles (NPs) are known to catalyze redox reactions as well as reactions that involve the nonoxidative dehydrogenation of alcohols and this motivated us to investigate the effects of Au deposited onto MgO-SiO_2.[34] The addition of Au increased the ethanol conversion and selectivity to 1,3-BD significantly (Figure 6). Au supported on magnesia-silica (50%MgO-

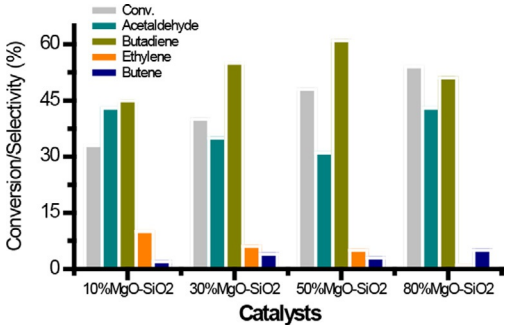

Figure 6. Effect of MgO loading on the activity and selectivity of ~3%Au/MgO-SiO_2 for the conversion of ethanol to 1,3-BD. Reaction conditions: T = 573 K, WHSV = 1.1 h^{-1}, Q_{tot} = 20 $cm^3 min^{-1}$, $P_{ethanol}$ = ~20 kPa, M_{cat} = 0.3 g.

SiO_2, Mg/Si = 2.6) has a sevenfold higher ethanol conversion and a sixfold higher 1,3-BD selectivity at 573 K than the catalyst that does not contain Au. Interestingly, the deposition of Au reduced the ethanol dehydration to diethyl ether or ethylene significantly. Notably, under similar reaction conditions, Au/SiO_2 showed a negligible ethanol conversion (~5%) and Au/MgO showed a moderate ethanol conversion (~25%) with acetaldehyde formed as the major product and only ~10% selectivity to 1,3-BD. Similarly, a physical mixture of Au/SiO_2 and MgO or Au/MgO and SiO_2 showed a significantly lower conversion and 1,3-BD selectivity than that obtained with Au dispersed on MgO-SiO_2 (Figure S4). These results illustrate the necessity to have the metallic, acidic, and basic sites in close proximity to realize a cooperative catalytic enhancement. Similarly, the introduction of Au on a magnesia-silica catalyst that contains the bulk MgO phase showed a much lower ethanol conversion and 1,3-BD selectivity (Figure S5). These results suggest that the formation of an amorphous MSH phase before or during the deposition of Au is essential to achieve a high activity and 1,3-BD selectivity.

The reaction temperature and feed contact time also affect the catalytic activity and selectivity to 1,3-BD. For instance, for Au supported on MgO-SiO_2, an increase of the reaction temperature from 523 to 573 K increased the conversion from 26 to 45%, but the 1,3-BD selectivity remained at ~60% (Figure 7). At 573 K, the catalyst productivity to 1,3-BD peaked

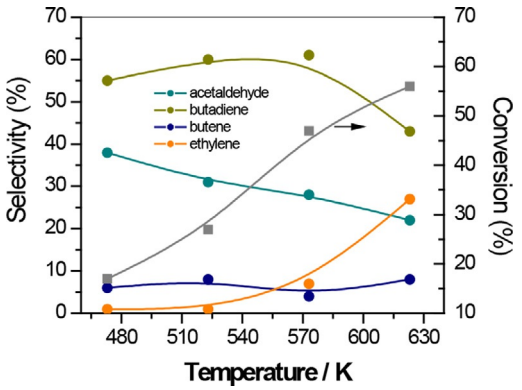

Figure 7. Effect of the reaction temperature on the conversion of ethanol to 1,3-BD over ~3%Au/50%MgO-SiO_2. Reaction conditions: T = 473-623 K, WHSV = 1.1 h^{-1}, Q_{tot} = 20 $cm^3 min^{-1}$, $P_{ethanol}$ = ~20 kPa, M_{cat} = 0.3 g.

at 0.135 $g_{1,3\text{-BD}}\, g_{catalyst}^{-1}\, h^{-1}$ at a WHSV of 1.1 h^{-1}. At temperatures above 573 K, ethanol dehydration to ethylene became dominant probably because of the increased acidity of the isolated hydroxyl groups present on the catalyst surface, which reduced the selectivity to 1,3-BD. On the basis of these results, we find that the use of the catalyst in the range of 533–573 K can achieve a high selectivity to butadiene at reasonable ethanol conversions. The major byproduct formed under these conditions is acetaldehyde, which can be separated and recycled back to the reactor.

The effects of the WHSV on the product distribution were explored for a wide range of values. In general, an increase of the WHSV (defined as the mass flow rate of ethanol divided by the weight of catalyst) led to a decrease in both the ethanol conversion and selectivity to 1,3-BD (Figure 8). Acetaldehyde

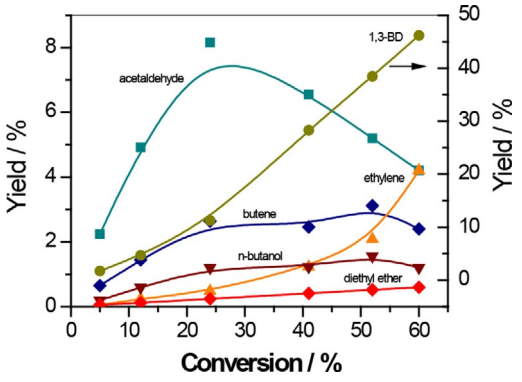

Figure 8. Dependence of product yields on ethanol conversion observed for the conversion of ethanol to 1,3-BD over ~3%Au/50%MgO-SiO_2 catalysts. Reaction conditions: T = 573 K, Q_{tot} = 20 $cm^3 min^{-1}$, $P_{ethanol}$ = ~20 kPa, M_{cat} = 0.3 g.

appeared at low ethanol conversions and passed through a maximum with the increasing conversion, which suggests that acetaldehyde is a primary product that undergoes secondary reactions through aldol condensation over acidic–basic sites. Remarkably, only trace quantities of crotonaldehyde and crotyl alcohol were detected under the reaction conditions

tested. Similarly, there was a clear lack of C_6 aldehydes that could have been formed by the cross-condensation of acetaldehyde with crotonaldehyde. C_6 aldehydes can undergo reduction and dehydration to form hexatrienes; however, these compounds were also absent from the products.[25] This evidence suggests strongly that the Meerwein–Ponndorf–Verley (MPV) reduction pathway of crotonaldehyde to crotyl alcohol and the subsequent dehydration over the acidic sites is rapid. The MPV reduction reaction of crotonaldehyde with ethanol is known to proceed over Lewis acid sites such as those present on MSH catalysts.[18,35] IR spectra of adsorbed pyridine showed the presence of very strong Lewis acid sites on magnesia-silicate, which suggests that the formation of these sites during the preparation of the magnesia-silica supports (e.g., the formation of the MSH phase) is responsible for the superior activity of the catalysts.

The dehydration of crotyl alcohol also occurs rapidly over our catalysts. We investigated the dehydration of crotyl alcohol with and without the cofeeding of ethanol using amorphous silica as the catalyst. The complete conversion of crotyl alcohol to 1,3-BD was observed irrespective of the presence of ethanol in the feed, which suggests that crotyl alcohol dehydration is rapid on the weakly acidic silanol groups ($pK_a = \sim 6–8$) present on silica. The dehydration of crotyl alcohol is favored greatly over the dehydration of ethanol to ethylene because of the presence of a double bond in crotyl alcohol, which stabilizes the cationic intermediate after the abstraction of protonated hydroxyl groups through an E1 mechanism.[5] Other major C_4 reaction byproducts formed over these catalysts are *n*-butanol and butenes. The selectivity to *n*-butanol increases as ethanol conversion increases. *n*-Butanol is likely formed by the transfer hydrogenation of crotyl alcohol with ethanol. Crotyl alcohol isomerizes to 1-buten-1-ol by the abstraction and relocation of the α-hydrogen atom to form the enol, which tautomerizes to *n*-butanal. A second transfer hydrogenation step (MPV reduction) then converts *n*-butanal to *n*-butanol.[34b] The formation of butenes in the reaction can be attributed to the partial hydrogenation of the 1,3-BD or the dehydration of *n*-butanol (Scheme 1).[25] The addition of H_2 to the feed had no effect on the formation of butenes, which suggests that butenes are not formed by the partial hydrogenation of 1,3-BD.

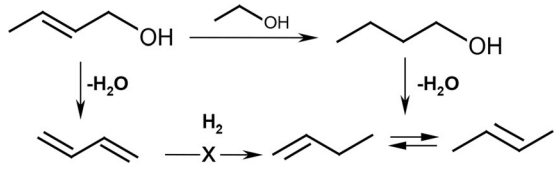

Scheme 1. Reaction pathway for the formation of butenes during ETB reactions.

A major side reaction in ETB reactions is the conversion of ethanol to diethyl ether and ethylene. The curve of ethylene selectivity versus the WHSV suggests that ethylene is a stable byproduct and that it is not involved in either oligomerization to give butenes or the Prins condensation with acetaldehyde

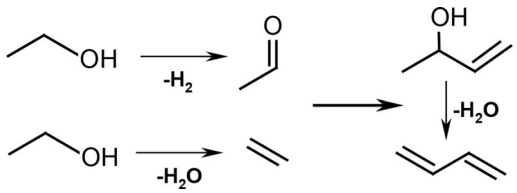

Scheme 2. Formation of 1,3-BD through a Prins condensation reaction pathway.

to give 1,3-BD (Scheme 2) as suggested by Fripiat et al.[36] The cofeeding of ethylene with ethanol did not improve the conversion of ethanol or the selectivity towards 1,3-BD. These results suggest that ethylene is not involved as an intermediate in 1,3-BD synthesis and support strongly the hypothesis that the self-condensation of acetaldehyde is the major pathway to 1,3-BD rather than the condensation of ethylene and acetaldehyde.

In light of the preceding discussion and consistent with previous studies, the mechanism of the conversion of ethanol to butadiene involves five critical steps: (a) acetaldehyde formation from ethanol by dehydrogenation; (b) aldol condensation of two acetaldehyde molecules to form an acetaldol; (c) dehydrogenation of acetaldol to crotonaldehyde; (d) MPV reduction reaction of crotonaldehyde with ethanol to form crotyl alcohol and acetaldehyde; and (e) dehydration of crotyl alcohol to form 1,3-butadiene (Scheme 3).[3,5,13,25] Ultimately, the selectivi-

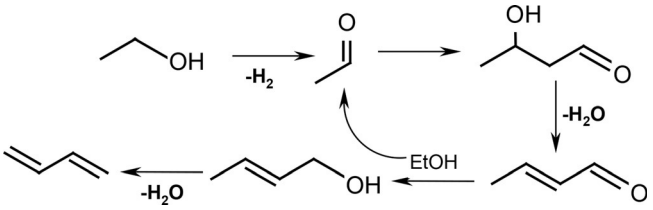

Scheme 3. Proposed mechanism for the conversion of ethanol to 1,3-BD.

ty of the reaction to 1,3-BD is affected strongly by the relative rates of reaction to various byproducts. Consequently, for a heterogeneous catalyst to achieve a high selectivity to 1,3-BD, it must have a subtle balance of acid–base and redox sites.

To support the proposed reaction mechanism, selected reaction intermediates were cofed with ethanol. It is well known that the addition of a small amount of acetaldehyde into the ethanol feed can increase the productivity to 1,3-BD significantly.[24] To examine this effect, acetaldehyde was cofed together with ethanol (molar ratio ethanol/acetaldehyde = 20), and the selectivity to 1,3-BD increased to ~75% at ~30% ethanol conversion at temperatures as low as 473 K (Figure S6). The other products formed were small amounts of butene and *n*-butanol (Scheme 1). The cofeeding of crotonaldehyde, another intermediate along the reaction pathway, produced an approximately 10-fold increase in the rate of 1,3-BD formation (Figure S7). These results suggest that the self-condensation of acetaldehyde is the rate-limiting step over the Au deposited on magnesia-silica catalysts. The apparent activation energy of

the ETB reaction calculated in the temperature interval of 333–353 K is 42 kJ mol^{-1}, consistent with the values reported for the aldol condensation of acetaldehyde over various metal oxide and mixed oxide catalysts.[37] Given that the activation energy for the ETB reaction is 42 kJ mol^{-1}, Au/MSH is three times more active than Ag/MgO-SiO_2 reported previously. The ability to work at 573 K rather than 673 K also lowers the selectivity to butenes. The lower production of butenes is very important from a practical point of view because the separation of butenes from butadiene is a very energy-intensive process, which leads to an increase in the GHG emissions for an ETB process. This result is also in agreement with the first-order dependence on acetaldehyde partial pressure, which suggests that enolate formation during the aldol condensation step is more critical than the C–C bond-forming step (Figure S7).

In situ IR spectroscopy was used to obtain additional information about the mechanism of 1,3-BD formation from ethanol over Au deposited on magnesia-silica. Upon passing pulses of ethanol over the catalyst at 473 K, an intense negative peak appeared at $\tilde{\nu}=3745$ cm^{-1}, which shows that ethanol interacts with the isolated silanol groups on the support silica surface. Peaks at $\tilde{\nu}=2985$ (methyl asymmetric stretching), 2935 (methyl symmetric stretching), and 2905 cm^{-1} (methylene asymmetric stretching) are characteristic of the ethyl groups of adsorbed ethanol (Figure S8).[38] A peak is also observed at $\tilde{\nu}=1680$ cm^{-1} that can be assigned to C=O vibrations in the product of ethanol dehydrogenation, acetaldehyde.[34,37] These results suggest that ethanol dehydrogenation proceeds by the activation of the alcohol O–H bond on the basic sites (Mg–OH) present on the surface of MSH and that coordinatively unsaturated sites on nearby Au NPs abstract the α-H (C–H bond activation) to form the aldehyde. The cleavage of an α-C–H bond is facilitated by the coordinatively unsaturated edge or corner atoms on the Au NPs.[34] An increase of the reaction temperature from 473 to 623 K resulted in a gradual disappearance of the peak at $\tilde{\nu}=1680$ cm^{-1} and the appearance of a peak at $\tilde{\nu}=1585$ cm^{-1}. The new feature is tentatively related to the formation of C=C bonds that arise from the aldol condensation of acetaldehyde and crotonaldehyde to form C_6 aldehydes or hexatrienes.[25] The appearance of C_6 aldehydes in the IR spectra but not in the reactor effluent suggest that a continuous flow of ethanol can limit the occurrence of this side reaction because ethanol acts as a hydrogen-transfer agent in the MPV reaction of crotonaldehyde to crotyl alcohol, which then dehydrates to 1,3-BD.

To confirm the role of basic sites in the ETB reaction over Au deposited on magnesia-silica catalysts, poisoning experiments were conducted by the co-feeding of propanoic acid with ethanol (Figure S9). The presence of acid in the reaction stream decreased the yield of acetaldehyde drastically, and the 1,3-BD yield became negligible after 1 h of time on stream. Upon the removal of propanoic acid from the feed, the ethanol dehydrogenation activity recovered but the selectivity to 1,3-BD remained almost 60% of that observed before the feeding of propanoic acid. This observation suggests that the basic sites involved in ethanol dehydrogenation are different from those responsible for aldol condensation and that the aldol condensation sites are more sensitive to the poisoning agent. On the basis of our CO_2 IR spectroscopy studies, we propose that weakly basic hydroxyl groups are responsible for dehydrogenation, whereas medium-to-strong Lewis acid–base sites (Mg–O pairs or O^{2-}) are responsible for aldol condensation. Notably, the co-feeding of pyridine with ethanol resulted in an improved yield to acetaldehyde but again to a decreased 1,3-BD yield. A similar observation has been reported previously and ascribed to the transfer of electronic charge from pyridine adsorbed on acidic sites to the nearest oxide anions, which thereby enhances their electron density.[20] This processes enhances the basicity of neighboring oxygen anion sites and hence their ability to participate in the dehydrogenation of ethanol to acetaldehyde. The subsequent removal of pyridine from the reactant stream resulted in the near-complete recovery of acetaldehyde yields; however, although the yield of 1,3-BD improved, it did not reach the same level obtained before the feeding of pyridine (Figure S9). These results suggest that aldol condensation occurs over strong-to-medium basic sites and that blocking these sites decreases the yield to 1,3-BD.

Process modeling and life-cycle analysis of GHG emissions

A process for the production of 1,3-BD from ethanol using the new catalyst was developed and simulated by using Aspen Plus. The purpose of this effort was to determine whether the production of 1,3-BD from ethanol could achieve lower GHG emissions relative to 1,3-BD produced from petroleum.

The process schematic is shown in Figure 9. Ethanol is vaporized and then heated to 523 K by heat exchange with the reactor effluent and steam. High-pressure steam is used to provide the heat of reaction and keep the reactor isothermal at 523 K. The reactor effluent passes through a series of heat exchangers and compressors so that liquid products can be re-

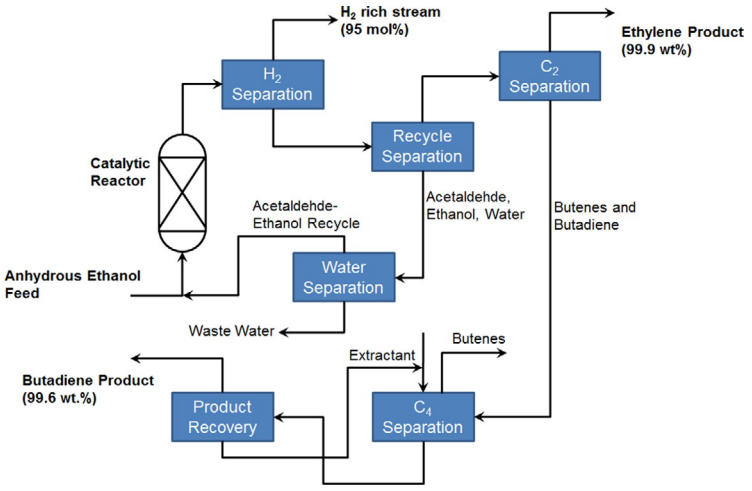

Figure 9. Simplified process flow diagram that depicts the various steps in the conversion of ethanol to 1,3-BD. Several of the heat integration/recovery schemes are omitted for simplicity.

covered. The separation of butadiene from the products of ETB is envisioned to involve the following steps: (a) Hydrogen separation from all the other products to yield a stream that contains 95 mol% H_2 with 3% ethylene and 2% C_4 alkenes and diene. (b) Ethylene and 1,3-BD along with butenes separation from the recycled heavies. (c) Ethylene separation from 1,3-BD to give a 99.5 wt% ethylene stream and a 98 wt% butadiene stream. (d) Recovery of polymer-grade (99.6 wt%) butadiene from the 98 wt% butadiene stream using a solvent extraction process with dimethylformamide as the solvent. (e) Separation of acetaldehyde and ethanol from the recycled heavies. The recycle stream contains some water (~5 wt%); however, in a continuous process, all the water produced in the reaction is separated and sent to a wastewater treatment process. The selected Au/MgO-SiO_2 catalyst can produce 1,3-BD with ~2% butenes, which thereby reduces the energy required for the separation of butenes from 1,3-BD considerably. Notably, although our catalyst gives some of the highest ethanol conversions and 1,3-BD selectivities reported in the literature, a commercial process would need to recycle the unreacted ethanol as well as the acetaldehyde formed in the process. Our experiments that involve the cofeeding of ethanol and acetaldehyde show that the addition of acetaldehyde improves the selectivity of the ETB reaction considerably and this is why acetaldehyde recycling is an important part of our process (Figure S6).

Aspen Plus was used to simulate and analyze the mass and energy flows in a 200 000 ton/year plant to produce 1,3-BD as an add-on to an existing ethanol production facility. The implementation of such a process in a Brazilian sugarcane biorefinery would use the excess heat and electricity produced by burning the bagasse. However, implementation in the USA close to a corn mill would most likely exploit the availability of cheap natural gas in a combined heat and power (CHP) system to provide the heat required for the separations and the electricity needed to run pumps, compressors, and various refrigeration loops. Our model showed that the process shown in Figure 10 could recover 0.55 $kg_{1,3\text{-}BD}\,kg_{ethanol}^{-1}$. In addition, the process could recover 0.014 $kg_{ethylene}\,kg_{1,3\text{-}BD}^{-1}$ as a coproduct. The heat demand for the plant was determined to be 6.18 $MJ\,kg_{1,3\text{-}BD}^{-1}$, and the electricity needed was 1.13 $MW\,kg_{1,3\text{-}BD}^{-1}$. A proportion of 32% of the heat demand was used to keep the system isothermal at 523 K, and the remaining 68% was used for product recovery. The process also produced 0.078 $kg_{95\%\ H_2\ stream}\,kg_{1,3\text{-}BD}^{-1}$. Such a stream would have applications in a petrochemical or refining complex; however, a standalone biorefinery would probably burn the H_2-rich stream for heat and electricity.

We used the process model shown in Figure 9 to investigate a set of scenarios and quantified the potential changes in the GHG emissions associated with a shift from petroleum-derived to bio-derived 1,3-BD. The analysis is based on three potential ethanol feedstocks: USA Midwest-grown corn grain, USA Midwest-grown corn stover, and Brazilian sugarcane. The scenarios include representative USA biorefineries located in Nebraska, Minnesota, Iowa, Indiana, and Illinois (Figure 10). Brazilian sugarcane ethanol is assumed to be imported by marine tanker into the port of Houston, one of the top ports for ethanol imports. In our scenarios, the proximity of the port of Houston to the petroleum infrastructure is a benefit.[39] USA-produced ethanol is assumed to be transported by rail, truck, and/or marine tanker. The locations of petroleum product shipping terminals, petroleum refineries, and ethane crackers, which convert ethane from natural gas liquids into ethylene and also yield 1,3-BD as a coproduct, are also shown in Figure 10. Our expectation is that the construction of ETB facilities in close proximity to petroleum refineries and ethane crackers would yield two primary benefits: (a) the hydrogen stream coproduced with 1,3-BD could be exported easily for use at petroleum refineries either by pipeline or other short-distance means of transportation; (b) the infrastructure necessary to store and transport ethylene and 1,3-BD would be readily available because most existing production is concentrated in that region; and (c) USA SBR manufacturing facilities are located primarily in Texas and Louisiana.[40] Although the majority of refineries and ethane crackers are located in Texas and Louisiana, a small number of facilities operate in the Chicago area; the ability to transport ethanol for conversion to 1,3-BD near these facilities could reduce the total transportation distance from 2300 km to approximately 300 km. Particularly in cases in which rail lines are congested and tanker trucks must be used for long-distance ethanol shipping, an optimization of the logistics could result in dramatic GHG emissions reductions. More details of input data and assumptions are provided in the Supporting Information.

The life-cycle GHG inventory results for petroleum-derived 1,3-BD and ethanol-derived 1,3-BD from corn grain, corn stover, and sugarcane using the Au supported on MSH catalyst are shown in Figure 11. The emissions for petroleum-derived 1,3-BD are calculated using an energy-content-based allocation of inputs to the ethylene production process. The model also includes energy and material inputs to the extractive distillation step required to produce a pure 1,3-BD stream from the crude C_4 coproduct of ethylene, which is typically 45–67%

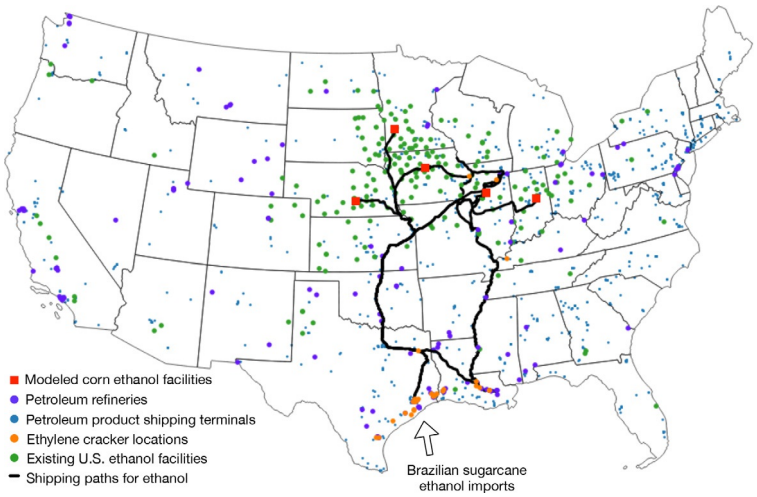

Figure 10. Logistics for ETB conversion.

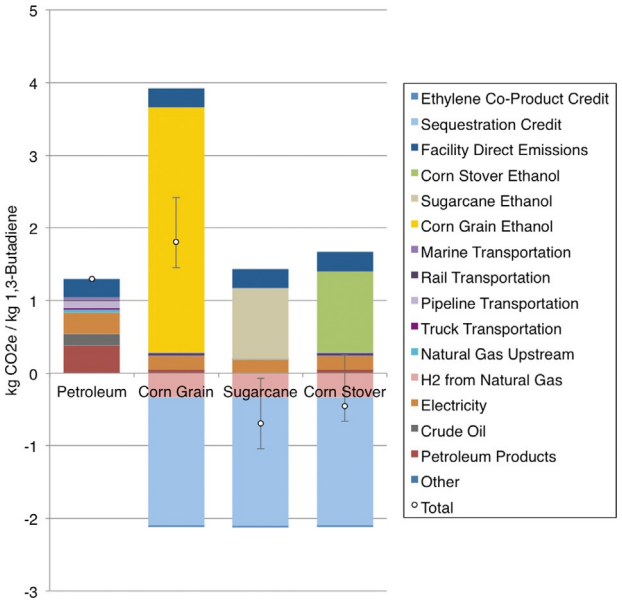

Figure 11. Life-cycle GHG Emissions per kg of 1,3-BD.

1,3-BD by weight. Unlike petroleum-derived C_4 fractions, our ETB process produces a 98% pure 1,3-BD stream that contains less than 2% butenes and no acetylenes, which results in a relatively less energy-intensive extraction process to reach 99.6% pure 1,3-BD (see Supporting Information for details). Although uncertainties associated with farming practices, biorefinery operations, and transportation distances/modes result in wide ranges, our analysis indicates that 1,3-BD produced from ethanol derived from sugarcane or corn stover is more attractive than petroleum-derived 1,3-BD even for the most pessimistic cases. For each ETB case, the GHG footprint of the ethanol inputs outweighs on-site energy demand as the single largest contributor to net GHG emissions, which indicates the importance of maximizing selectivity and conversion. The two largest contributors to net sequestration (or emissions avoidance) are hydrogen exports, which we assume offset natural-gas-derived hydrogen production at petroleum refineries, and 1,3-BD end-of-life biogenic carbon sequestration associated with noncombustion applications for used rubber. We chose to explore only scenarios in which hydrogen could be exported to petroleum refineries or other facilities that require a relatively pure hydrogen stream. The coproduct credit that results from the export of hydrogen is far greater than the potential for on-site emission reductions through hydrogen combustion for process heat (Figure 11). Thus, the colocation of ETB facilities with facilities able to make use of the hydrogen stream is preferable to the production of 1,3-BD at biorefinery locations at which hydrogen would need to be combusted on-site in place of natural gas.

In each case, our model is based on the assumption that 1,3-BD is used for SBR production and ultimately incorporated into automotive tires. At the end-of-life, approximately 44% of tire material is combusted and the remainder is repurposed (32.2%), recycled (1.8%), and landfilled (22%).[41] Landfilling or otherwise not combusting petroleum-derived 1,3-BD avoids fossil emissions, and the same end-of-life practices result in the sequestration of biogenic carbon in the cases for which bio-based ethanol is the feedstock. Although the GHG footprint of corn grain ethanol is too large to be fully offset by this form of carbon sequestration, 1,3-BD derived from both sugarcane and corn stover is a net carbon-negative product (Figure 11). The fossil emissions that result from petroleum-derived 1,3-BD combustion are included in the facility direct emissions in Figure 11. Very recently, Cespi et al. suggested that the Lebedev single-step process has a lower economic and environmental burden than the conventional naphtha cracking route and is a more valuable alternative than the Ostromislensky process.[42] Compared to petroleum-based 1,3-BD, which has a GHG footprint of 1.3 kg_{CO_2} $kg_{1,3\text{-}BD}^{-1}$, 1,3-BD derived from corn grain ethanol increases emissions by 39–40% in the average case but may only increase emissions by 12% in the most optimistic case. 1,3-BD derived from sugarcane ethanol decreases emissions by 150% in the average case, and 1,3-BD derived from corn stover ethanol decreases emissions by 140% in the average case.

The results of our process analysis indicate that, as long as SBR continues to be recycled or repurposed in noncombustion applications, the production of 1,3-BD from ethanol derived from sugarcane or corn stover can reduce atmospheric CO_2 concentrations. Conversely, the production of 1,3-BD from corn grain ethanol will likely increase net GHG emissions even in the most optimistic cases, which indicates that the selection of low-carbon ethanol sources is key to achieve net climate benefits. However, these results do not include indirect land use change, which is highly uncertain but potentially significant. The analysis also suggests that integration with existing infrastructure is crucial. In cases in which a facility produces valuable coproducts that may be challenging to transport, such as hydrogen, the location of facilities near points of demand can facilitate large coproduct credits. Our study shows that after we have developed a technology, for example, a new or improved catalyst for ethanol conversion to 1,3-BD, a detailed analysis is necessary to determine the conditions necessary to reduce GHG emissions relative to existing petroleum routes.

Conclusions

A new catalyst is reported for the one-step conversion of bioethanol to 1,3-butadiene (1,3-BD) in high yields. The most active and selective catalyst is Au supported on MgO dispersed on silica (MgO-SiO_2). Notably, during calcination MgO is converted completely to a hydrated magnesium silicate. The formation of a magnesium silicate hydrate phase, the ratio between acid and base components, the nature and concentration of redox sites, and the type of silica used for the support and the conditions of its pretreatment were all found to play a crucial role to define the activity and selectivity of MgO-SiO_2-supported Au. Studies of the reaction mechanism confirmed that 1,3-BD formation from ethanol involves (a) dehydrogenation of ethanol to produce acetaldehyde by a process that involves both weakly basic sites on the magnesia-silicate and redox sites present on the surface of Au nanoparticles; (b) aldol condensa-

tion of two acetaldehyde molecules to crotonaldehyde, which occurs over the medium-to-strong basic sites present on the surface of the dispersed magnesia-silicate; (c) Meerwein–Ponndorf–Verley reduction of crotonaldehyde with ethanol over Lewis acidic Mg sites to produce crotyl alcohol and acetaldehyde; and (d) dehydration of crotyl alcohol to 1,3-BD over the mildly acidic silanol groups on the support surface. The high catalytic activity and selectivity of the MgO-SiO_2-supported Au reported here is a direct consequence of the proper balance between the redox, basic, and acidic sites on the catalyst surface.

We also show that the one-step conversion of ethanol to 1,3-BD can be implemented in a biorefinery to yield high-purity 1,3-BD in addition to hydrogen and ethylene as coproducts with a relatively low on-site energy demand. If the modeled ethanol to 1,3-BD facilities are sited to take advantage of the existing petrochemical infrastructure in the USA, which includes hydrogen demand by petroleum refineries, ethanol-derived 1,3-BD can achieve dramatic reductions in net greenhouse gas emissions.

Experimental Section

Catalyst preparation

Catalysts that contained various loadings of MgO (MgO loading = 10–80 wt%, Mg/Si = 0.15–6) on a silica gel support (SiO_2 = Silicycle, BET_{SA} = 230 $m^2 g^{-1}$) were prepared by incipient-wetness impregnation using magnesium nitrate as the magnesium precursor. The catalysts were dried at 373 K overnight and then calcined in air at 823 K for 3 h. A modified DP method using urea as the precipitating agent was used to deposit Au on the MgO-SiO_2 samples. An aqueous solution of $HAuC_{l4}$ was prepared and added to 1 g of MgO-SiO_2 support. Urea was added until the pH of the solution was nearly 8–10. The material was then stirred for 15 min at RT and subsequently for 1 h at 333 K. The material was aged for 3 h, and the solid was recovered by filtration. This material was washed with a copious amount of water to remove Cl^- ions, and the resulting yellowish solid product was then dried overnight in a vacuum oven at 373 K. A final reduction at 623 K in H_2 for 2 h produced the Au (5–6 nm from TEM analysis) doped MgO-SiO_2 catalyst used for further study.

Characterization

The metal content was determined by using inductively coupled plasma optical emission spectroscopy (ICP-OES) conducted at Galbraith Laboratories (Knoxville, TN). IR spectra were acquired by using a Thermo Scientific Nicolet 6700 FTIR spectrometer equipped with a liquid-nitrogen-cooled mercury cadmium telluride (MCT) detector. Each spectrum was obtained by averaging 32 scans taken with 1 cm^{-1} resolution. The catalyst (0.05 g) was pressed into a 20 mm diameter pellet (< 1 mm thick) and placed in a custom-built transmission cell equipped with CaF_2 windows, a K-type thermocouple for temperature control, and resistive cartridge heaters. N_2 adsorption isotherms were performed by using a Micromeritics Gemini VII surface area and pore volume analyzer. The specific surface area and pore size were calculated using the BET and Barrett–Joyner–Halenda (BJH) equations.

Solid-state ^{29}Si MAS NMR spectra were obtained by using a Bruker Avance I 500 MHz spectrometer equipped with a H/X double resonance magic-angle spinning probe that used 4 mm O.D. rotors. The ^{29}Si with ^{1}H decoupling MAS NMR spectra were acquired at 99.37 MHz by using a ^{29}Si 908 pulse width of 7.5 ms, recycle delay of 600 s, and spinning rate of 10–11 kHz. All ^{29}Si NMR spectra were referenced against polydimethyl siloxane at $\delta = 22$ ppm (relative to TMS at $\delta = 0$ ppm). The resolution obtained in the ^{29}Si NMR spectra was sufficient for accurate peak assignments, and the relative peak area of each site was obtained by curve-fitting using a series of Gaussian peaks.

Au nanoparticle sizes were determined from images taken by using bright-field transmission electron microscopy (BF-TEM) by using an FEI Tecnai T12 electron microscope operated at a 120 kV accelerating voltage. The elemental composition of the support material was determined by STEM-EDS. Elemental mapping by STEM-EDS was performed by using an FEI Titan electron microscope located at the Molecular Foundry at the Lawrence Berkeley National Laboratory. The microscope was operated at an accelerating voltage of 200 kV, and fluorescent X-rays with energies between 0–40 kV were collected by using a four-segment silicon drift detector. The catalyst composition was quantified using the Bruker Esprit software program with the Cliff–Lorimer method using the $O_{K\alpha}$ (0.525 keV), $Mg_{K\alpha}$ (1.254 keV), $Si_{K\alpha}$ (1.739 keV), and $Au_{K\alpha}$ (9.713 keV) peaks.

Reaction studies

The gas-phase ETB reaction was performed in a 6.35 mm OD (~4 mm ID) quartz tube that contained an expanded section (~12.7 mm OD, ~20 mm length). The reactor was packed with quartz wool above and below the catalyst bed to hold the catalyst in place. Ethanol was injected into the He flow by using a syringe pump. The catalysts were pretreated in He at 473 K for 2 h before contact with the feed. Experiments were performed at 473–623 K, total gas pressures of 1 atm, and a total gas flow rate of 20 $cm^3 min^{-1}$. All the results reported were obtained after 200 min of time on stream. Reaction products were analyzed by using an Agilent 6890N gas chromatograph equipped with a bonded and cross-linked (5%-phenyl) methyl polysiloxane capillary column (Agilent, HP-1) connected to a flame ionization detector.

Acknowledgements

This work was supported by the Energy Bioscience Institute. This work was part of the DOE Joint BioEnergy Institute (http://www.jbei.org) supported by the U.S. Department of Energy, Office of Science, Office of Biological and Environmental Research, through contract DE-AC02-05CH11231 between Lawrence Berkeley National Laboratory and the U. S. Department of Energy. STEM-EDS mapping was performed at the National Center for Electron Microscopy at the Molecular Foundry, Lawrence Berkeley National Laboratory. Work at the Molecular Foundry was supported by the Office of Science, Office of Basic Energy Sciences, of the U.S. Department of Energy under Contract No. DE-AC02-05CH11231. Prof. John Myers from the University of Wyoming is acknowledged for his advice and help in developing the process model. We gratefully acknowledge the contributions of Dr. Chris Canlas, Dr. Gregory Johnson, and Dr. Jason Wu to the characterization section of the manuscript.

Keywords: biomass · alcohols · gold · magnesium · supported catalysts

[1] D. R. Dodds, R. A. Gross, *Science* **2007**, *318*, 1250 – 1252.
[2] G. W. Huber, S. Iborra, A. Corma, *Chem. Rev.* **2006**, *106*, 4044 – 4098.
[3] a) E. V. Makshina, M. Dusselier, W. Janssens, J. Degreve, P. A. Jacobs, B. F. Sels, *Chem. Soc. Rev.* **2014**, *43*, 7917 – 7953; b) G. O. Ezinkwo, V. P. Tretyakov, A. Aliyu, A. M. Ilolov, *ChemBioEng Rev.* **2014**, *1*, 194 – 203; c) J. M. R. Gallo, J. M. C. Bueno, U. Schuchardt, *J. Braz. Chem. Soc.* **2014**, *25*, 2229 – 2243.
[4] C. H. Christensen, J. Rass-Hansen, C. C. Marsden, E. Taarning, K. Egeblad, *ChemSusChem* **2008**, *1*, 283 – 289.
[5] W. Janssens, E. V. Makshina, P. Vanelderen, F. De Clippel, K. Houthoofd, S. Kerkhofs, J. A. Martens, P. A. Jacobs, B. F. Sels, *ChemSusChem* **2015**, *8*, 994 – 1008.
[6] C. White, *Chem.-Biol. Interact.* **2007**, *166*, 10 – 14.
[7] S. V. Lebedev, *Russ. J. Gen. Chem.* **1933**, *3*, 698 – 708.
[8] J. Ostromislenskiy, *J. Russ. Phys. Chem. Soc.* **1915**, *47*, 1472 – 1506.
[9] W. M. Quattlebaum, W. J. Toussaint, J. T. Dunn, *J. Am. Chem. Soc.* **1947**, *69*, 593 – 594.
[10] *Encyclopedia of Chemical Processing and Design, Vol. 5* (Ed.: J. J. McKetta), **1977**, pp. 146 – 147.
[11] *Butadiene Sales Specifications*, The Dow Chemical Company, March **2012**.
[12] Prices of commodities, Independent Commodity Information Service, **2015**, http://www.icis.com.
[13] C. Angelici, B. M. Weckhuysen, P. C. A. Bruijnincx, *ChemSusChem* **2013**, *6*, 1595 – 1615.
[14] a) C. Angelici, M. E. Z. Velthoen, B. M. Weckhuysen, P. C. A. Bruijnincx, *ChemSusChem* **2014**, *7*, 2505 – 2515; b) C. Angelici, F. Meirer, Ad. M. J. van der Eerden, H. L. Schaink, A. Goryachev, J. P. Hofmann, E. J. M. Hensen, B. M. Weckhuysen, P. C. A. Bruijnincx, *ACS Catal.* **2015**, *5*, 6005 – 6015.
[15] A. D. Patel, K. Meesters, H. den Uil, E. de Jong, K. Blok, M. K. Patel, *Energy Environ. Sci.* **2012**, *5*, 8430 – 8444.
[16] Y. Kitayama, A. Michishta, *J. Chem. Soc. Chem. Commun.* **1981**, 401 – 402.
[17] Y. Kitayama, M. Satoh, T. Kodama, *Catal. Lett.* **1996**, *36*, 95 – 97.
[18] S. Kvisle, A. Aguero, R. P. A. Sneeden, *Appl. Catal.* **1988**, *43*, 117 – 131.
[19] R. Ohnishi, T. Akimoto, K. Tanabe, *J. Chem. Soc. Chem. Commun.* **1985**, 1613 – 1614.
[20] H. Niiyama, S. Mori, E. Echigoya, *Bull. Chem. Soc. Jpn.* **1972**, *45*, 655 – 659.
[21] Y. Kitayama, K. Shimizu, T. Kodama, S. Murai, T. Mizusima, M. Hayakawa, M. Muraoka, *Stud. Surf. Sci. Catal.* **2002**, *142*, 675 – 679.
[22] M. D. Jones, C. G. Keir, C. D. Iulio, R. A. M. Robertson, C. V. Williams, D. C. Apperley, *Catal. Sci. Technol.* **2011**, *1*, 267 – 272.
[23] E. V. Makshina, W. Janssens, B. F. Sels, P. A. Jacobs, *Catal. Today* **2012**, *198*, 338 – 344.
[24] V. V. Ordomskiy, V. L. Sushkevich, I. I. Ivanova, WO 2012/015340A1, **2012**.
[25] V. L. Sushkevich, I. I. Ivanova, V. V. Ordomsky, E. Taarning, *ChemSusChem* **2014**, *7*, 2527.
[26] a) D. R. M. Brew, F. P. Glasser, *Cem. Concr. Res.* **2005**, *35*, 85 – 98; b) T. Zhang, C. R. Cheeseman, L. J. Vandeperre, *Cem. Concr. Res.* **2011**, *41*, 439 – 442.
[27] J. Temuujin, K. Okada, K. J. D. MacKenzie, *J. Solid State Chem.* **1998**, *138*, 169 – 177.
[28] Y. Sun, Y. Xia, *Science* **2002**, *298*, 2176 – 2179.
[29] J.-B. d'Espinose de la Caillerie, M. Kermarec, O. Clause, *J. Phys. Chem.* **1995**, *99*, 17273 – 17281.
[30] G. Vigil, Z. Xu, S. Steinberg, J. Israelachvili, *J. Colloid Interface Sci.* **1994**, *165*, 376 – 382.
[31] J. I. Di Cosimo, V. K. Diez, M. Xu, E. Iglesia, C. R. Apesteguia, *J. Catal.* **1998**, *178*, 499 – 510.
[32] T. De Baaerdemaeker, M. Feyen, U. Muller, B. Yilmaz, F.-S. Xiao, W. Zhang, T. Yokoi, X. Bao, H. Gies, D. E. De Vos, *ACS Catal.* **2015**, *5*, 3393 – 3397.
[33] O. M. Busch, W. Brijoux, S. Thompson, F. Schuth, *J. Catal.* **2004**, *222*, 174 – 179.
[34] a) S. Shylesh, D. Kim, C. Ho, J. Wu, G. R. Johnson, A. T. Bell, *ChemSusChem* **2015**, *8*, 3959 – 3962; b) C. R. Ho, S. Shylesh, A. T. Bell, *ACS Catal.* **2016**, *6*, 939 – 948.
[35] G. Natta, R. Rigamonti, *Chim. Ind.* **1947**, *29*, 239 – 243.
[36] V. Gruver, A. Sun, J. J. Fripiat, *Catal. Lett.* **1995**, *34*, 359 – 364
[37] J. E. Rekoske, M. A. Barteau, *Ind. Eng. Chem. Res.* **2011**, *50*, 41 – 51.
[38] V. L. Sushkevich, I. I. Ivanova, E. Taarning, *ChemCatChem* **2013**, *5*, 2367 – 2373.
[39] 2014 Ethanol Exports and Imports, **2015**, Renewable Fuels Association. http://www.ethanolrfa.org/page/-/rfa-association-site/studies/2014%20U.S%20Export-Import%20Report.pdf?nocdn=1.
[40] Economic Impact Analysis for the Polymers and Resins Group INESHAP Revised Draft Report, **1995**, U.S. Environmental Protection Agency. http://www.epa.gov/airtoxics/pr1/eiapr1.pdf.
[41] Carbon Footprint of USA Rubber Tire Recycling **2007**, Institute for Environmental Research and Education, **2009**, http://www.cmtirerecyclingequipment.com/Public/14864/FinalRubberTireRecyclingCarbonFootprint.pdf.
[42] D. Cespi, F. Passarini, I. Vassura, F. Cavani, *Green Chem.* **2016**, *18*, 1625 – 1638.

Received: February 15, 2016
Revised: March 22, 2016
Published online on May 19, 2016